Three dimensional numerical simulations of the liquid transfer between a cavity and a moving roll

Diego M. Campana*, Sebastián Ubal, Maria D. Giavedoni and Fernando A. Saita
Instituto de Desarrollo Tecnológico para la Industria Química (INTEC-CONICET-UNL), Güemes 3450, CP3000, Santa Fe, República Argentina. Phone: +54-343-4559175 (Ext. 2172).
*Email: dcampana@santafe-conicet.gov.ar

Marcio S. Carvalho
Department of Mechanical Engineering, Pontifícia Universidade Católica do Rio de Janeiro, Rua Marques de Sao Vicente 225 (Gavea), Rio de Janeiro, RJ, 22451-900, Brazil. Phone: +55-21-35271174.
Email: msc@puc-rio.br

Presented at the 17th International Coating Science and Technology Symposium
September 7-10, 2014.San Diego, CA, USA

Extended Abstract:

In last years, the development of novel conductive organic materials together with the need to build electronic circuits on flexible substrates has renewed the attention on printing technologies (Willmann et al (2014)). The effort has been specially directed to roll-to-roll procedures (R2R), mainly due to its high production rates. In addition, roto-gravure techniques can give the solution to reach the compromise between production rate and the required printed pattern resolution (Krebs, 2009). In roto-gravure printing, the pattern to be printed is engraved on the surface of a rotating roll; then, as depicted in figure 1-a, the printing is made by pressing the flexible substrate between the engraved and a second soft roll (Dodds et al. (2009)).

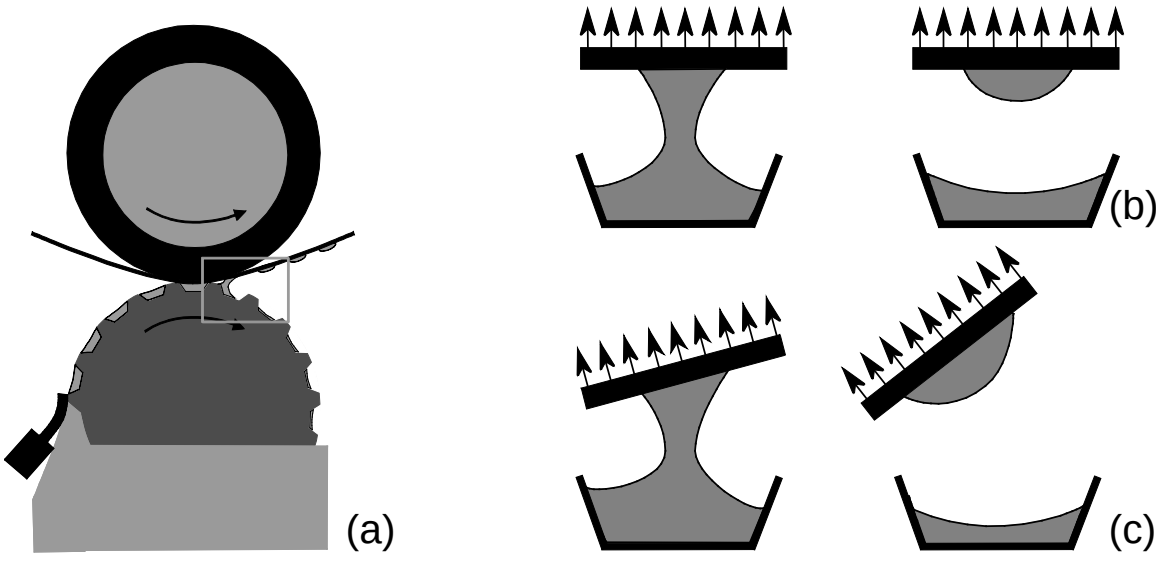

Figure 1: (a) Sketch of a roto-gravure printing system; (b) simpler model for the liquid transfer between a single cavity and substrate, considering a one dimensional surface motion; (c) a more realistic model, where the surfaces motion tends to mimic the roll-to-roll kinematics.

The understanding of the liquid transfer between cavities and moving substrates has been the focus of some recent researches. Dodds (2011) made 2D axisymmetric simulations of the liquid transfer between a fixed single trapezoidal cavity and a surface moving away in one direction (see figure 1-b), to calculate the pick-out liquid fraction φ, that is defined as the relation between the liquid volume extracted from the cavity and the initial liquid volume. Dodds (2011) mainly explored the effect of wettability (contact angles) and geometry of the cavity on the fraction φ. He found that the cavity aspect ratio has an important influence of the liquid transfer process. Later, Campana and Carvalho (2014)) solved a similar model but introducing a more complex kinematic model of the surfaces motion which mimics a R2R configuration, as shown in figure 1-c. They found that the relative rotational and shearing velocities between the cavity and substrate surfaces improve the emptying and increase the fraction φ, respect to the simpler one directional motion. Also, for low capillary numbers, it was observed that liquid squeezes out the cavity into the outer plane surface, before capillary forces could break the fluid filament. In those cases, the problem changes to a liquid bridge being stretched between two plane surfaces and the fraction φ ~ 0.5. Campana and Carvalho (2014)) only solved planar cavities (grooves) using the R2R kinematics. Thereby, the azimuthal curvature of the liquid bridge -which dominates the evolution and breakup of the filament at later stages of the transfer- was not considered. Since most of the printed patterns are built by using 3D trapezoidal cavities (dots), the applicability of those results are limited. Thus, this work is an extension of Campana and Carvalho (2014), where the focus is to solve a full 3D problem. The new model does not have symmetry restrictions and this makes possible to compute the liquid emptying in situations more similar to the real cases. Next we briefly describe its main characteristics.

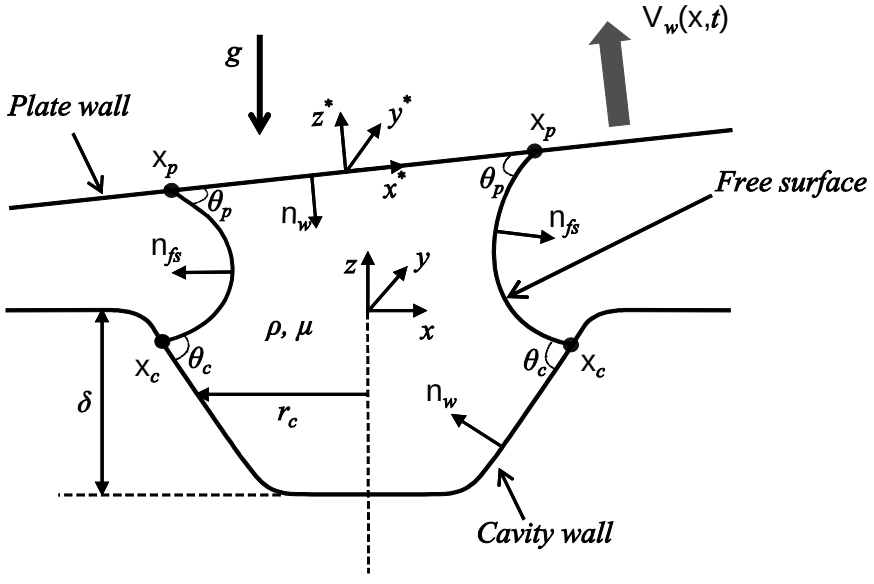

Figure 2: Sketch of the transversal section (*z-x* plane) of the flow domain, showing spatial variables, dimensions and geometric parameters. The coordinate system (*x, y, z*) is fixed at the center of the cavity surface while (x^*, y^*, z^*) is the frame attached to the moving plate.

Figure 2 represents the cross section (in the *z-x* plane) of the three-dimensional domain considered to model the liquid transfer between a single cavity and a moving plate. The trapezoidal cavity, with depth δ,

is perfectly symmetric under a z-axis rotation; however, because the plate has a relative velocity $V_w(\mathbf{x}, t)$ respect to the fixed (x, y, z) frame with components in z and x directions, the liquid bridge is not symmetric. The expression of $V_w(\mathbf{x}, t)$ was derived in detail in Campana and Carvalho (2014). At $t = 0$, the plate is located perfectly horizontal over the cavity at $z = H_0$. Also a t=0, the origin of the second frame (x^*, y^*, z^*) attached to the moving plate has coordinates x^*= 0, y^*= 0 and z^*= H_0. This frame will be used later to represent the printed pattern on the substrate.

We consider the fluid as Newtonian with density ρ, viscosity μ and surface tension σ, all of them being constant. At $t = 0$, the system is in equilibrium and a static meniscus is formed between the cavity and the plate with static contact angles θ_c and θ_p, respectively, while x_p and x_c are the curves representing the contact lines. The outer gas phase has negligible density and viscosity (relative to the liquid properties) and a constant pressure $p_0 = 0$ which it is taken as reference. Thus, by neglecting inertial and gravity effects, the flow is modelled with the continuity and Stokes equations. Regarding the boundary conditions, on the free surface the capillary forces act only in the normal direction and at contact lines we consider constant contact angles which are independent on contact line velocity. Also, we used Navier boundary conditions on solid walls to remove the stress singularity close to the contact lines (with slip coefficient β). Finally, solid walls are impervious and fluid has the same normal velocity as the solid surface.

As discussed in Campana and Carvalho (2014), the parameters governing the model are: the capillary number $Ca = \mu V_E / \sigma$, where $V_E = \omega R \sqrt{(10/R_b)}$ is an extensional velocity, R the roll radius and ω its angular velocity; $R_b = R/\delta$ is the dimensionless roll radius and $\omega_b = \omega \delta / V_E \sim 1/ R_b^{1/2}$ is a kinematics parameter of the model. The contact angles θ_c and θ_p must be also specified and finally, the trapezoidal cavity shape is approximated by a continuous hyperbolic tangent function, with parameters r_c and r_s (see Campana and Carvalho (2014)).

The system was discretized with the Galerkin finite elements method (FEM) on a moving mesh which follows the domain deformation via an Arbitray Lagrangian-Eulerian formulation. Sprittles and Shikmurzaev (2013) present a detailed explanation of the method used to impose the boundary conditions and kinematics restrictions via Lagrange multipliers. This method was successfully used by Campana and Carvalho (2014) and here it was extended to the 3D case. Details on geometry definitions, initialization of the solution and re-meshing stages when the mesh becomes excessively distorted are similar to those explained in Campana and Carvalho (2014). To choose and appropriate refinement close to the contact lines, we monitor the differences between the imposed and calculated contact angles. With the selected element sizes, those differences were always below 10% and usually around 1%. Also, mass conservation was checked during all simulation, and was typically achieved with 0.1% of error.

To check the validity and behavior of the 3D model, we first obtained solutions for the 2D axisymmetric models. In this case, we used a one-dimensional simplification of the full kinematic, where V_w has component only in z-direction. As in Campana and Carvalho (2014), we selected the following set of parameters: R = 0.15 m, δ = 50 μm and ω = 13 /s (R_b = 15240 and ω_b = 2.5 x 10^{-3}), $\theta_c = \theta_p = 70°$, r_c = 0.8 and r_s = 0.3. The simulations are stopped when the minimum filament radius reaches an imposed

limit r_l = 0.05; in this work we consider that smaller values of r_l lead to the breakup of the filament. Also, from the computations we got z_l, that is the z-coordinate corresponding to r_l, and the liquid volume above z_l; this quantity, divided by the initial volume, is assumed to be the liquid fraction φ transferred to the plate. Figure 3 shows the fraction φ for several values of *Ca*. It can be observed that for the axisymmetric model, φ diminishes monotonically as *Ca* is decreased. This behavior was explained in detail in Campana and Carvalho (2014), by analyzing the mobility of the contact lines (in cavity and plate) as a function of the capillary pressure gradient. Interfacial shapes as well as values of φ computed with the 3D model for the same simplified kinematic (plate displacing only in z-direction), were in excellent agreement with those computed with the axisymmetric model. Thus, the full 3D model was successfully validated.

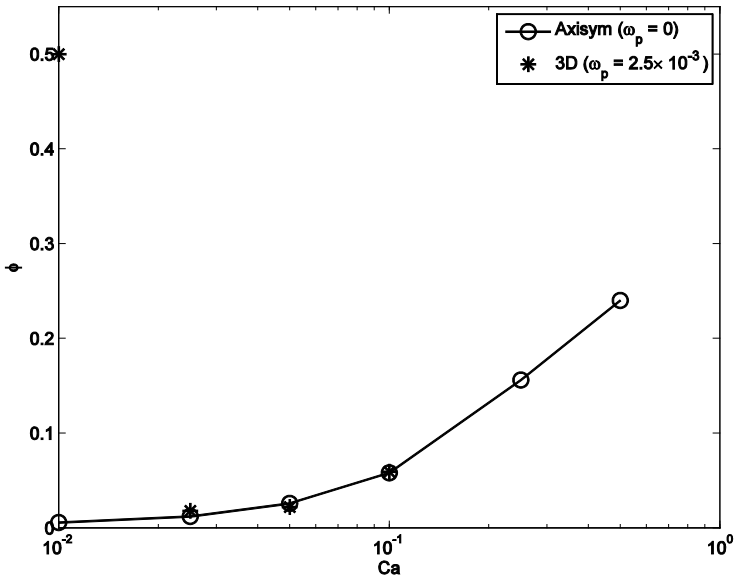

Figure 3: Transferred liquid fraction φ versus *Ca*. Open circles + line correspond to 2D axisymmetric model and asterisk to results of the full 3D model.

Thereupon, we obtained 3D results for the full R2R kinematics and calculated the corresponding values of φ; those results are also included (asterisks) in figure 3 and they show just small differences with the 2D axisymmetric predictions for *Ca* > 0.02. However, we observed larger differences for smaller *Ca*; in particular at *Ca* = 0.01, where the 3D model predicts φ = 0.5. This behavior can be explained with the help of figure 4, which shows a sequence of images of the cavity emptying for *Ca* = 0.01. It can be observed how the kinematics promotes a squeezing of the fluid outside the cavity until the exterior plane surface ($t \leq 2.8$). At this stage, the evolution continues as a liquid bridge being stretched between two plane surfaces and the breakup occurs almost symmetrically (at t ~5.0).

While this result predicts more efficiency in both cavity emptying and liquid transfer at low *Ca*, it also implies a higher slipping of the pattern on the substrate, which could diminish the fidelity of the printing pattern. To show this, figure 5 depicts the contact lines on the substrate close to breakup. Note that graphs were plotted on (x^*, y^*) axis, that is, on the frame attached to the moving substrate. In this frame,

the pattern must be ideally centered on $x^* = y^*=0$ (cross mark) for good pattern fidelity. However, a higher shift is observed when *Ca* is decreased.

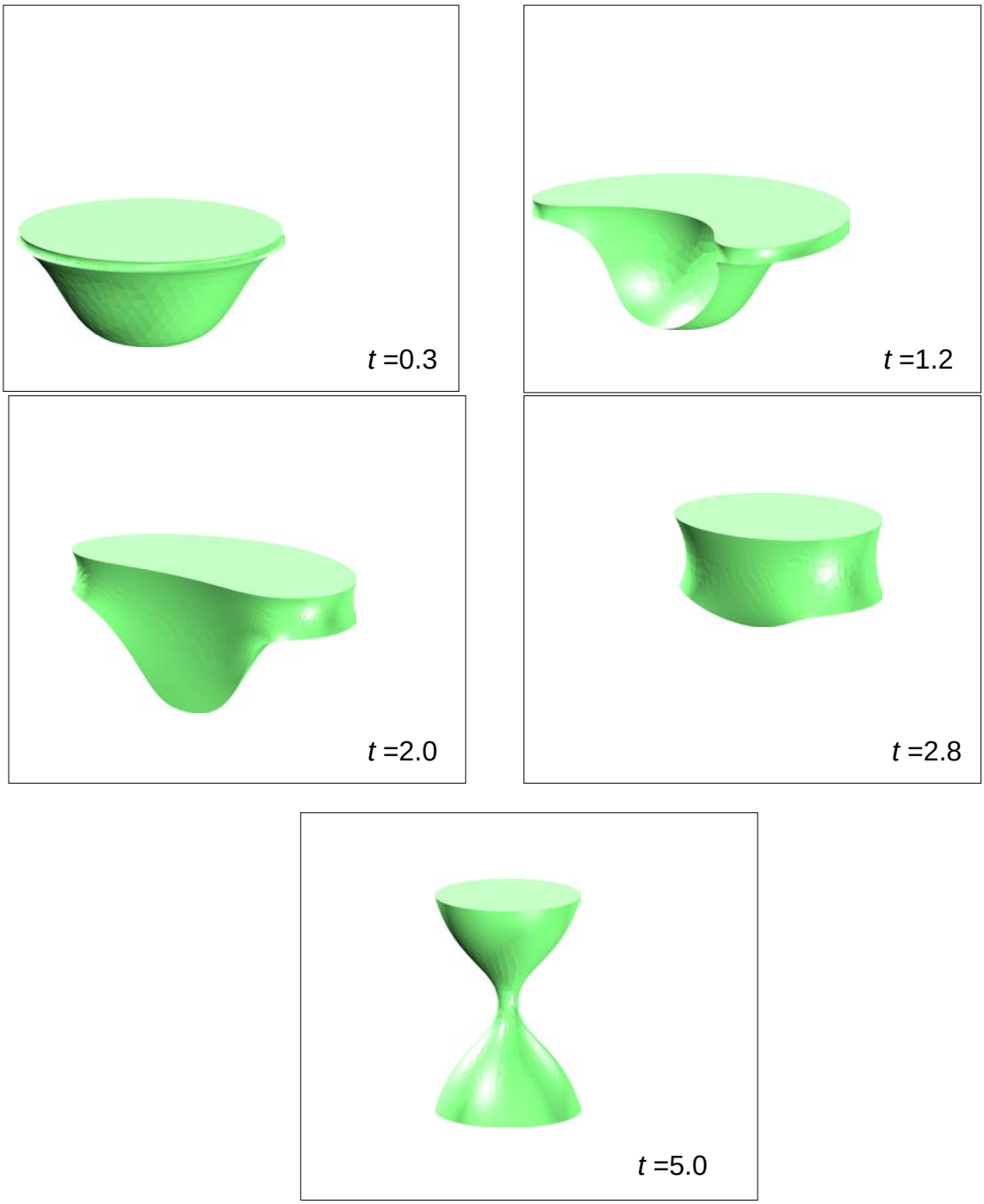

Figure 4: Evolution of the liquid transfer for *Ca* = 0.01. At *t* = 2.8 the liquid spreads almost completely outside of the cavity. Then, the dynamics is very similar as filament stretching between parallel plates and the breakup occurs almost symmetrically (φ ~ 0.5) at *t* ~5.0.

In summary, these results predict that liquid transfer would be more efficient at high values of *Ca*, because both higher transfer fraction and pattern fidelity should be attained. While at smaller values of *Ca* the fraction φ could be also high, the strong slipping of contact lines could make the printed pattern unacceptable. At present more simulations are being performed to capture the transition of φ versus *Ca* (at low *Ca*) and an experimental setup is being prepared to corroborate these numerical predictions.

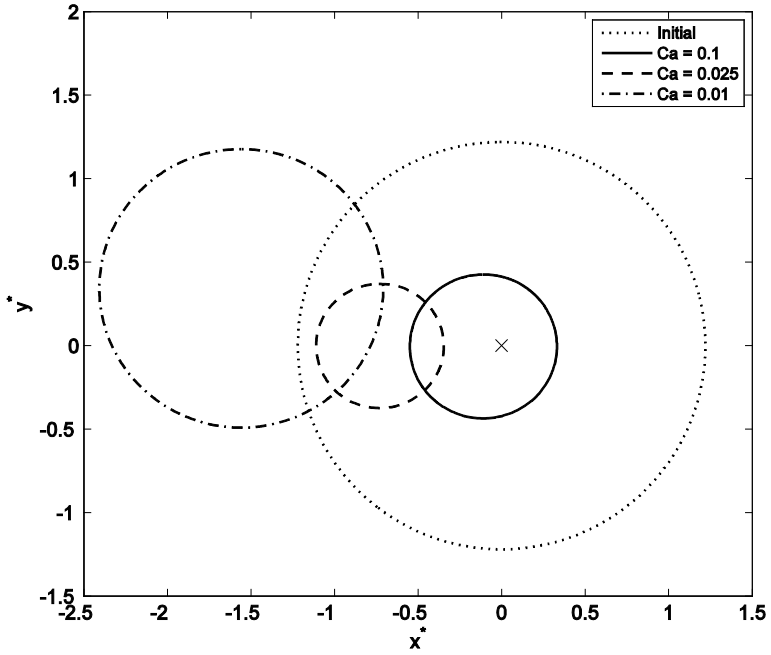

Figure 5: Contact line on the moving substrate, plotted versus the moving frame (*x*, y**). The curve denoted as "Initial" represents the position of the contact line at at *t* = 0 all simulations, while the others correspond to the breakup time for indicated *Ca*.

References

Campana, D. M. and Carvalho, M. S. Liquid transfer from single cavities to rotating rolls. *J. Fluid Mech*., 747, 545-571, 2014.

Dodds, S., Carvalho, M. & Kumar, S. Stretching and slipping of liquid bridges near plates and cavities. *Physics Fluids*, 21, 092103, 2009.

Dodds, S. Stretching and slipping liquid bridges: Liquid transfer in industrial printing. *PhD Thesis, University of Minnesota*, 2011.

Krebs, F. Fabrication and processing of polymer solar cells: A review of printing and coating techniques. *Solar Energy Materials & Solar Cells*, 93, 394–412, 2009.

Sprittles, J. E. and Shikhmurzaev, Y. D. Finite element framework for describing dynamic wetting phenomena. *Intl J. Numer. Meth. Fluids* 68, 1257–1298, 2012.

Willmann, J., Stocker, D., Dörsam, E. Characteristics and evaluation criteria of substrate-based manufacturing. Is roll-to-roll the best solution for printed electronics? *Organic Electronics: physics, materials, applications*. 15(7), 1631-1640, 2014.